Design and Validation of a Low-Cost Triaxial 5G RF-EMF Exposure Sensor

Jeroen Van der Straeten, Han Van Bladel, Kenneth Deprez, Wout Joseph, *Senior Member, IEEE*, and Günter Vermeeren

***Abstract*—A low-cost monitoring network, to measure radio frequency (RF) electromagnetic field (EMF) exposure induced by 5G, is required for risk communication and to support research into long-term health and ecological effects related to 5G technologies. A low-cost triaxial fifth generation (5G) RF-EMF exposure sensor was designed, calibrated, and validated in the field, using a commercial network. The sensor uses a triaxial antenna-based measurement design and is able to measure the exposure induced by 5G communication in the n78 (3300–3800 MHz) and the n77 (3300–4200 MHz) frequency band up to 3900 MHz. The sensitivity of the simultaneous analog-to-digital converter (ADC)-based triaxial sensor is 0.06 V/m, while having a combined uncertainty u_c of 3.12 dB. The sensor was tested indoor and in two outdoor environments (private and commercial 5G networks). The maximum measured electric-field level induced by 5G (n77 band) was 0.89 V/m [500 m from a commercial base station (BS)] and 2.87 V/m (60 m from a private BS), which are 1.5% and 4.8% of the International Commission on Non-Ionizing Radiation Protection (ICNIRP) guidelines, respectively. A second measurement campaign was used to compare the values of the electric field captured by the novel triaxial 5G sensor and commercial measurement equipment (SRM-3006). The average values of the electric field registered by the triaxial 5G sensor differ on average 2.8 dB from the values of the SRM-3006, which is within the measurement uncertainty of the SRM-3006.**

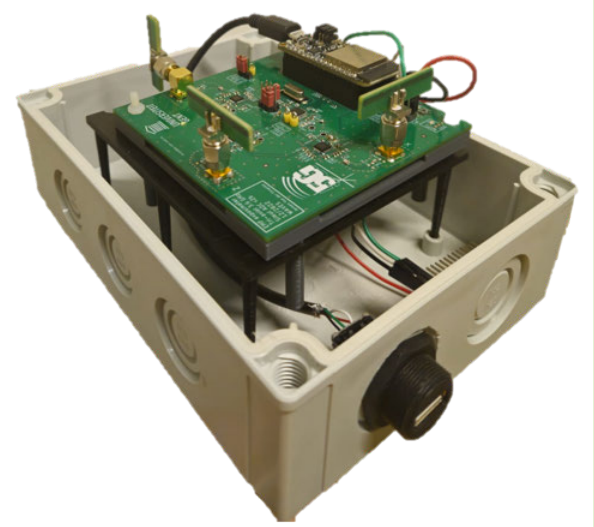

***Index Terms*—Fifth generation (5G), radio frequency (RF) electromagnetic fields (EMFs), RF exposure, root mean square (rms) power detector, simultaneous sampling, triaxial.**

I. Introduction

THE fifth generation (5G) of telecommunication networks is currently the latest standard. 5G introduced the usage of new frequency bands such as n77 (3300–4200 MHz) with subbands n48 (3550–3700 MHz), and n78 (3300–3800 MHz) [1]. The carrier frequencies and used bandwidths are higher compared to the carrier frequencies used in previous generations of telecommunication networks (2G–4G), which raised public concerns that the signals, more specifically the power of the electromagnetic fields (EMFs) induced by 5G communication, could have adverse health effects [2], [3], [4] or ecological effects [5]. The radio frequency (RF)-EMF exposure can be measured with the use of RF-EMF exposimeters [6], [7], [8], [9] or spectrum analyzer setups [10], [11], [12]. The latter uses an antenna, with known characteristics, which is connected to the spectrum analyzer that measures the received power level. Subsequently, the power levels are converted into *E*-field (electric field) values [13].

On a large scale static or dynamic monitoring networks are used to measure RF-EMF exposure [14], [15]. This article focuses on the design of a low-cost 5G sensor that could be used to deploy low-cost monitoring networks. A low-cost monitoring network, to measure RF-EMF exposure induced by 5G is required, to support research focusing on these topics and for risk communication. As discussed by Deprez et al. [16], a modular design can be used to measure the RF-EMF exposure induced by four telecommunication wireless network technologies (GSM, UMTS, LTE, 5G) operating at different

Received 10 February 2025; accepted 3 March 2025. Date of publication 14 March 2025; date of current version 1 May 2025. This work was supported in part by the European Union's Horizon Europe Research and Innovation Program [5G expOsure, causaL effects, and rIsk perception through citizen engagement (GOLIAT)] under Grant 101057262. The associate editor coordinating the review of this article and approving it for publication was Dr. Wei Tang. *(Corresponding author: Jeroen Van der Straeten.)*

The authors are with the Department of Information Technology, INTEC-WAVES, Ghent University/imec, 9052 Ghent, Belgium (e-mail: jeroen.vanderstraeten@ugent.be).

Digital Object Identifier 10.1109/JSEN.2025.3549631

frequencies. These sensors use a single dipole antenna to measure the RF-EMF exposure induced by a selected frequency band, which is insufficient to measure all three vector components of the EMF. The sensors described by Deprez et al. use a dedicated RF-front end, consisting of low noise amplifiers, off-the-shelf bandpass filters, and power detectors, to monitor exposure induced by a selected frequency band.

Software-defined radios (SDRs) are also used to measure RF-EMF exposure [16], [17], [18], [19]. SDR-based sensors implement the tasks of the analog components (filters, mixers, amplifiers, and so on) via software rather than dedicated hardware. This has advantages and disadvantages. The sensors are often more compact and could also give frequency information, e.g., to identify the frequencies that generate the most RF-EMF exposure. The disadvantages of SDRs-based sensors are the price and limited bandwidth. 5G uses radio channels up to 100 MHz [frequency range 1 (FR1)]. This requires SDRs with large bandwidth or a sequential measurement routine to be able to monitor the whole radio channel [19]. For the second method, the SDR would divide the radio channel into subchannels and combine the sequentially obtained results. Sârbu et al. [18] also proposed techniques to perform real-time triaxial measurements by combining three SDRs or three spectrum analyzers, which requires expensive equipment, making it unsuitable for a large-scale monitoring network.

Several RF-EMF monitoring networks already exist in Europe [14], e.g., *Observatoire des ondes* in France and Belgium operated by Exem and the Agence Nationale des Fréquences (ANFR) [20], [21], [22], *emf ratel* [23] in Serbia operated by the Regulatory Authority for Electronic Communications and Postal Services, *monitor-emf* [24] in Romania operated by The National Authority for Management and Regulation in Communications (ANCOM) and two networks in Greece; National Observatory of EMFs (NOEF) [25] operated by the Greek Atomic Energy Commission (EEAE) and *Pedion24* [26] operated by four Greek university laboratories. However, not all of them are able to measure the RF-EMF exposure induced by 5G (frequency band n77). Because: 1) the sensors do not cover the frequency range; e.g., the *Pedion24* network measures up to 3 GHz [26]; and 2) the sensors measure the total *E*-field over a wide frequency (e.g., 0.1 MHz–7 GHz) [23], [24], [25] but, these sensors are unable to determine the frequency band responsible for a certain level of exposure.

The existing sensor networks mentioned above use the AMB-8059 [27] (manufactured by Narda Safety Test Solutions), except for the *Observatoire des ondes* project, which uses a custom-made sensor designed by Exem [20], [22].

The AMB-8059 [27], [28] is a commercially available RF-EMF sensor or broadband area monitor (manufactured by Narda Safety Test Solutions) with a frequency range of 10 Hz–60 GHz. The sensitivity and the frequency range of the area monitor depend on the isotropic probe connected to the AMB-8059. A quad-band probe [28] is used in [23], [24], [25], and [26], measures three mobile services (EGSM 900, EGSM 1800, UMTS) and also provide a wideband measurement from 0.1 MHz up to 7 GHz. The lowest sensitivity of the probes used by the AMB-8059 is 0.2 V/m, with the corresponding resolution of 0.01 V/m and anisotropy of ±0.8 dB.

Different commercial sensors such as the MonitEM [29] (from wavecontrol) also exist. The sensor is similar to the AMB-8059 [27]; isotropic triaxial probes, frequency range from 10 Hz to 60 GHz depending on the probe [30]. The sensitivity, resolution, and anisotropy information is not available in the (public) datasheet [30]. However, commercial sensors such as the AMB-8059, MonitEM, etc. are more expensive than the previously discussed hardware sensors [16] and SDRs, but often achieve higher accuracy and/or reliability.

The current state-of-the-art low-cost sensors—hardware- or software-based—use a single antenna, i.e., measure along a single axis and thus only measure a single component of the *E*-field which increases the uncertainty of the results, or lack the capabilities to monitor RF-EMF exposure induced by the newly introduced frequency band (n77; 3300–4200 MHz) used for 5G. Therefore, this article discusses a novel 5G triaxial sensor design that could be used to bridge the gap in low-cost 5G RF-EMF exposure monitoring. The new design was developed, manufactured, calibrated, and finally tested indoors (in an office) near a commercial 5G base station (BS) and outdoors near a private and commercial 5G BS. The contributions of this article are: 1) triaxial measurements, i.e., measure along three axes at the same time; 2) enabling the use of higher sample rates; 3) adding expansion capabilities, e.g., SD card storage; and 4) in situ validation of the triaxial sensor.

II. Methods and Materials

A. Design

Fig. 1(a) shows the triaxial 5G RF-EMF exposure sensor, which is assembled in a weatherproof enclosure made from polycarbonate (IP 66/67; Fibox). The triaxial EMF exposure sensor uses three dipole antennas, which are positioned perpendicular to each other. The dipole antennas resonate at 3.86 GHz and have a −10 dB bandwidth of 800 MHz. The signal is first passed through an off-the-shelf multilayer bandpass filter (by TDK) before being measured by a root mean square (rms) power detector (HMC1120LP4E; Hittite now Analog devices) [31]. The voltage at the output of the rms detector is a linear-in-dB representation of the received RF signal power. The rms power detector is capable to measure the power of RF signals within a frequency range of dc to 3.9 GHz while having a dynamic range between 62 and 68 dB. The lower detector limit is frequency dependent and ranges between −60 and −57 dBm. The analog output of the rms detector ranges from 0.32 to 2.7 V and is converted by a four-channel simultaneous-sampling (SS)-analog-to-digital converter (ADC). The measurements are processed by an ESP32 which is present on the Adafruit HUZZAH32 development board. The ESP32 is a 240 MHz dual-core microcontroller (Tensilica Xtensa LX6) with 520 kB of SRAM. The ESP32 also supports Bluetooth v4.2 and WiFi 802.11 b/g/n. The latter is used to transmit processed measurement data to a server, which ensures time synchronization. An expansion header is also present on the printed circuit board (PCB) of the sensor, to add other features such as

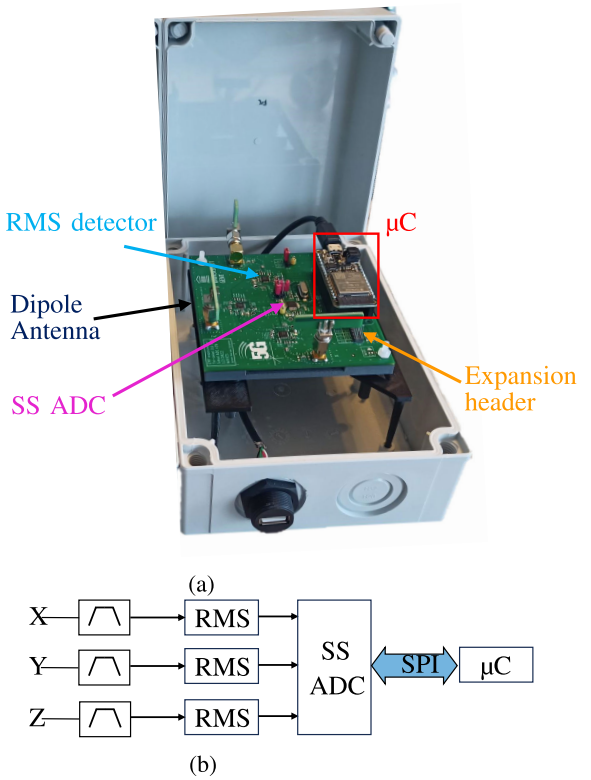

Fig. 1. (a) SS-ADC-based triaxial EMF sensor assembled, on a 3-D printed support structure, installed in a weatherproof enclosure. (b) Sensor concept; the sensor uses three dipole antennas, three multilayer bandpass filters, three rms detectors, and one SS-ADC. The microcontroller uses SPI to communicate with the ADC.

TABLE I
RELATION BETWEEN 5G FR1 SUBCARRIER SPACINGS AND OFDM SYMBOL DURATIONS [1], [32]

Subcarrier Spacing [kHz]	15	30	60
OFDM Symbol Duration [μs]	66.67	33.33	16.67
OFDM Symbol Duration including cyclic prefix [μs]	71.35	35.68	17.84
ADC Shortest sampling interval [μs]	7.82		

local data storage (micro-SD card), a real-time clock, or for debugging purposes. The triaxial sensor concept is shown in Fig. 1.

The serial peripheral interface (SPI) communication protocol is used to interface with the SS-ADC. The SS-ADC is a four-channel SS delta-sigma ADC with a programmable resolution (16 or 24 bit), gain amplifier, and sample rate up to 128 ksps. This ADC was chosen because it can measure all three components of the E-field at the same time and the *high* sample rate makes it theoretically possible to measure the exposure related to individual 5G OFDM symbols. The duration of a 5G OFDM symbol depends on the configuration of the subcarrier spacing (see Table I). A larger subcarrier spacing results in shorter OFDM symbol durations [1], [32]. The sensor is powered with an external 5 V power supply via the USB connector. A basic 5V/1A power adapter (HC105 [33]; manufactured by Ansmann) or a 5 V power bank (Xtorm ac Power Bank Pro 41.600 mAh) were used during testing.

B. Processing

The sensor utilizes an ESP32, a dual-core microcontroller, to interact with the SS-ADC, and to perform the required processing. The use of both cores enables higher sample rates and more advanced processing. The ESP32 requires real-time operating systems (RTOSs) to utilize both cores. The RTOS is also used to schedule multiple tasks on the same core (see Table II). The triaxal sensor has a measurement period of 1 s. The first 800 ms are used to perform measurements. The last 200 ms are foreseen to transmit or store the data. The dual-core implementation makes it possible to read and convert the data in parallel. Minimum, maximum, and average measured rms power per channel are calculated by the microcontroller during the **convertData** task. The powers are transmitted or stored during the **sendTask**. During postprocessing, the power data P [dBm] is converted to power density S [W/m^2]

$$S = \frac{P}{\mathrm{AF}} \tag{1}$$

where antenna factor (AF) is the AF, which is determined experimentally, and finally to E-field values with Z_0 the free-space impedance [34]

$$E = \sqrt{SZ_0}. \tag{2}$$

The E-field values per channel i are sum squared to acquire the total E-field exposure

$$E_{\mathrm{tot}} = \sqrt{\sum_i {E_i}^2}. \tag{3}$$

The aforementioned postprocessing could also be performed by the microcontroller of the sensor.

Table II lists the tasks that are scheduled and performed by the microcontroller of the triaxial sensor.

The **SensorConfig** and **CreateInterrupts** tasks are executed only once, but still need to be scheduled to lock the corresponding subprocesses (e.g., interrupt handlers) to core 1. Core 0 is mainly used by the **spiReadData** task. This choice was made to prevent read errors caused by task switching or interrupts. The triaxial sensor prototype was able to achieve a sample rate of 32 ksps at a resolution of 16 bits. This corresponds to a total data throughput of 2.5 Mbit/s. A higher resolution could be selected but requires more processing and would impact the maximum achievable sample rate of the sensor.

C. Calibration

The sensors are calibrated to ensure accurate exposure measurements. The calibration procedure consists of two steps, an on-board and free-space calibration. The sensitivity and dynamic range of the sensors are determined during the on-board calibration. Subsequently, during the free-space calibration, the relation between the measured power and RF-EMF exposure level is characterized.

1) On-Board Calibration: For the on-board calibration, the antennas are disconnected and replaced by 50-Ω terminations. Each channel, one at a time, of the triaxial exposure sensor is connected to a calibrated signal generator (SMB100A;

TABLE II

TASKS OF THE MICROCONTROLLER OF THE TRIAXIAL SENSOR. EACH TASK RUNS ON CORE 0 OR CORE 1 AND IS EXECUTED ONCE (1x) OR RUNS PERPETUALLY (∞). TASK SCHEDULING IS REQUIRED TO BE ABLE TO USE BOTH CORES OF THE MICROCONTROLLER

Task name	Runs	Core	Task info
SensorConfig	1x	1	First the RMS detectors are configured and started. Next the sample rate, internal reference, and dynamic range of the SS-ADC are set. The task will also start the other tasks.
CreateInterrupts	1x	1	This task starts a hardware timer (period 200 ms) and configures the external interrupt. The hardware timer is used to ensure a fixed measurement duration. The external interrupt is used to register the conversion state of the SS-ADC. The external interupt will alert the **spiReadData** task.
spiReadData	∞	0	This task uses SPI to interact with the ADC. The task waits for an external interrupt generated by the ADC, receives raw data from the ADC, converts the raw data to a voltage, and then adds the voltage data to a queue (*convertQueue*). The queue is used to pass data between the two cores.
convertData	∞	1	This task pulls data form the *convertQueue* and translates it to a received power level based on a lookup table. Next, the minimum, maximum, and average received power level, for the different axes, are calculated and passed to the **sendTask**.
sendTask	∞	0,1	This task takes care of the wireless communication connection between the sensor and the server. This task can also be used to transmit the data via the extension port.

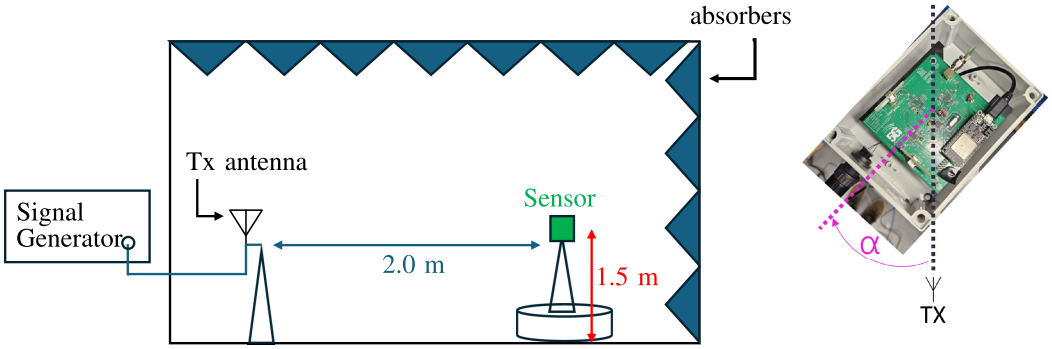

Fig. 2. Free-space calibration setup. The triaxial sensor is mounted on a tripod, which is positioned on a turn table. The angle of arrival α indicates the relative orientation between the sensor and the transmitter. The triaxial sensor is installed at a height of 1.5 m and the distance to the horizontal polarized antenna is 2.0 m. The setup is located in a semi-anechoic chamber. The goal is to measure the AF and to characterize the isotropic behavior of the sensor. (a) Sensor setup. (b) Angle of arrival.

manufactured by Rohde and Schwarz) to determine the output voltage of the RF detector as a function of the incident power. The output power of the signal generator is swept from −70 to 8 dBm in steps of 1 dBm at a fixed frequency of 3.625 GHz (center frequency of the n48 frequency band). Next, the output power of the signal generator is set to −20 dBm and the frequency is swept from 200 MHz to 4 GHz, in steps of 50 MHz, to verify the attenuation of the multilayer bandpass filter.

2) Free-Space Calibration: Fig. 2(a) shows the setup used to perform the free-space calibration of the sensor. The triaxial sensor [see Fig. 1(a)] is mounted on a tripod, which is placed on a calibrated turn table (model: TT 0.8 PF; manufactured by Maturo GmbH). Vertical and horizontal polarized antennas are used to transmit a 3.625 GHz signal (generated by SMB100A) toward the sensor sequentially. The sensor is placed at a height of 1.5 m and the distance from the transmit antenna to the sensor is 2.0 m. The setup is placed in a semi-anechoic chamber. The turn table is used to perform two full rotations at an angular velocity of 2°/s. Next, the triaxial sensor is replaced by an isotropic frequency-selective EMF strength analyzer (SRM-3006; manufactured by Narda Safety Test Solutions [35]). The analyzer is used to measure the strength of the EMFs at 3.625 GHz (with an uncertainty of ±3 dB) [36]. The outcome is then used to calculate the AF of the antennas used to measure the different components of the E-field. Finally, the isotropic behavior is characterized.

3) Frequency Verification Test: The fully calibrated sensor is verified using a frequency sweep from 3300 to 3800 MHz in steps of 25 MHz (n78 frequency band). The sensor was mounted on a tripod in a semi-anechoic chamber. The orientation or position of the sensor remained fixed during this test. The frequency was swept in 5 s increments, during which the sensor performed five measurements. Next, the aforementioned procedure was repeated using the SRM-3006. The goal is to compare the performance of the triaxial sensor and the SRM-3006 for the n78 frequency band, which is used in Belgium.

D. Energy Consumption

Energy consumption is an important economic and ecological aspect when developing a sensor. The energy consumption is measured using an Energy meter (E305EM5; manufactured by Perel). The Energy meter has a sensitivity of 0.1 kWh and 0.1 W, making it only suitable when performing long-term measurements. The energy consumption is monitored for six days. The sensor was powered by a 5 V/1 A power adapter (HC105; manufactured by Ansmann).

E. In Situ Measurements: Configuration

Measurements of 5G signals were performed indoors and outdoors with the triaxial sensor. The indoor tests were conducted in an office building in Ghent, Belgium (commercial

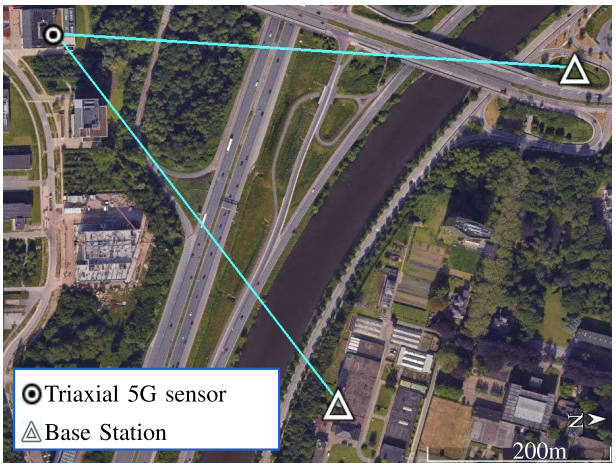

Fig. 3. Indoor measurement; the triaxial sensor (circle) was installed on the fifth floor, next to a window, on the north side of an office building in Ghent. The BSs are represented by a triangle.

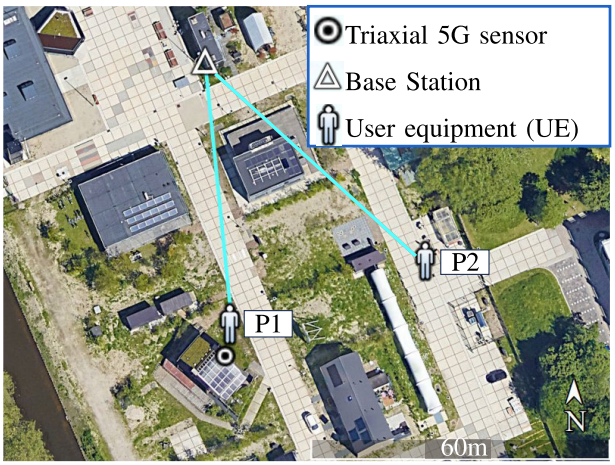

Fig. 4. First outdoor measurement campaign; the triaxial sensor (circle) was installed in the Green Village in Delft, The Netherlands. The distance to the BS (triangle) in both scenarios is 60 m. First, the user (person) is generating artificial traffic in position 1 ($P1$) and later the user moves to position 2 ($P2$), whilst the sensor position remains fixed. Both positions are in LOS of the BS.

5G network). The sensor was installed next to a window in a room on the 5th floor located on the north side of the building, 500 m to the nearest BS (see Fig. 3).

The first set of outdoor tests was conducted in the Green Village in Delft, The Netherlands [16]. This location was chosen due to the presence of a private 5G BS, which could be used to generate artificial traffic at a center frequency of 3.85 GHz and corresponding bandwidth of 100 MHz. The goal is to measure the difference in exposure when the positions of the triaxial sensor, user equipment (UE), and BS are collinear ($P1$ in Fig. 4) and when they are not ($P2$ in Fig. 4). This configuration was chosen such that the sensor and UE are not in the same beam during the tests conducted in $P2$. The distance between the sensor and the BS is 60 m. Both positions are in the line of sight (LOS) of the BS. The artificial traffic consists of a 6-min download test conducted by a UE (Crosscall Core-Z5).

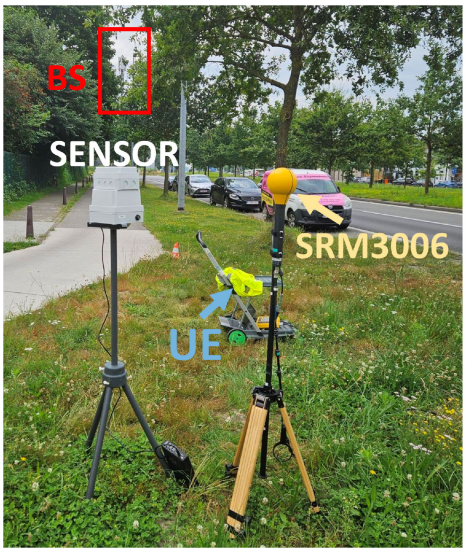

Fig. 5. Second outdoor measurement campaign; The triaxial sensor (SENSOR) is installed next to the antenna of the SRM-3006. A UE (Samsung S23) is positioned in front of the sensor and the SRM-3006, to generate 5G traffic. The triaxial sensor, UE, and BS are collinear.

The second outdoor test (see Fig. 5) is conducted at a large roundabout in Ghent, Belgium (51.01133°N, 3.70407°E). The SRM-3006 (frequency-selective EMF measurement device [35]; manufactured by Narda Safety Test Solutions, here considered as "golden standard") was installed at a distance of 1 m to the triaxial sensor, and measured concurrently. The triaxial sensor and the antenna of the SRM-3006 are positioned at a height of 1.5 m. The distance between the triaxial sensor and the BS (nonstandalone, dual telecom operators) is 90 m. A UE (Samsung S23) is used to download a 10-GB file over 5G. The SRM-3006 performs 5-s measurements, at a center frequency of 3.65 GHz, bandwidth of 300 MHz, and resolution bandwidth of 1 MHz. During the measurements, a laptop was used to control and change the settings and modes of SRM-3006 automatically via Python. The results obtained with the triaxial sensor and the SRM are compared.

III. Results

A. Calibration

1) On-Board Calibration: The on-board calibration of the SS-ADC-based sensor concluded the similarity of the behavior of all three orthogonal components (x, y, and z), $\Delta V(P_{in}) = \pm 0.05\,V$ (see Fig. 6). The Z component of the triaxial sensor has a noise floor (NF) of -60.73 dBm which is the lowest of all axes ($P_{x,\mathrm{NF}} = -55.73$ dBm and $P_{y,\mathrm{NF}} = -57.73$ dBm). The onboard calibration data is used to construct a lookup table, which is used to perform the on-sensor data conversion and later for postprocessing.

2) Free-Space Calibration: The free-space calibration is used for the characterization of NF of the sensor, which is 0.06 V/m. Signals transmitted by the horizontally polarized calibration antenna were mainly captured by both horizontal oriented antennas (x-axis and z-axis) of the triaxial sensor, as expected. Signals transmitted by the vertical polarized

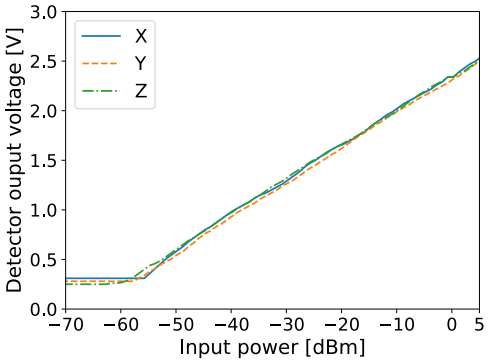

Fig. 6. On-board calibration results; all components of the sensor show a similar log-linear relation. The Z component has the lowest NF of -60.73 dBm.

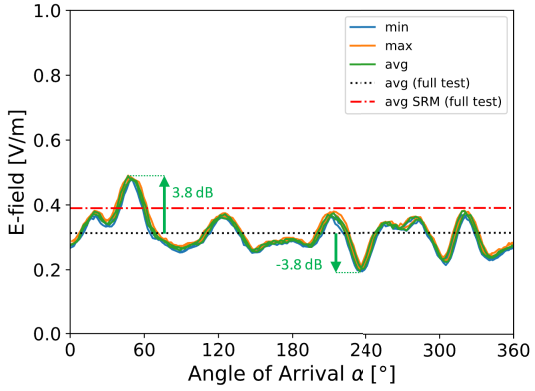

(a)

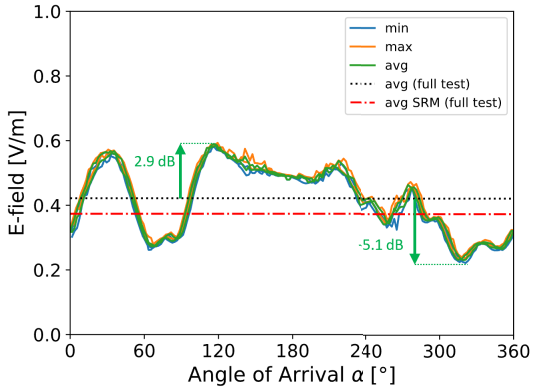

(b)

Fig. 7. Free-space calibration of the sensor; the isotropic performance depends on the polarization of the transmit antenna. (a) Horizontally polarized TX. (b) Vertically polarized TX.

antenna were mainly captured by the vertical oriented antenna (along the y-axis) of the triaxial sensor. The measurements also provide information about the isotropy of the sensor. Fig. 7 shows a maximum anisotropy of ± 3.8 dB for a horizontally polarized transmit antenna (TX) and $+2.9/-5.1$ dB for a vertically polarized TX. The standard deviation (σ) of the average measured E-field value is 0.006 V/m for both TX polarisations. The average E-field value reported by the triaxial sensor is within 3 dB of the E-field value reported by the SRM,

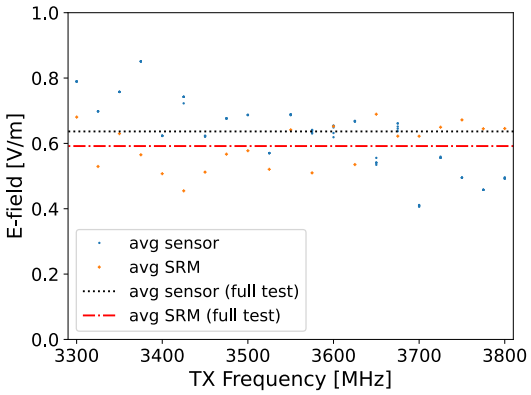

Fig. 8. Frequency test; the performance of the sensor was compared to the performance of the SRM-3006. The average E-field reported by both devices for the full test differs by 0.03 V/m. The sensor performed five measurements for each frequency.

i.e., the uncertainty range of the SRM-3006. Degradation of the isotropic performance of the sensor could be caused by the microcontroller socket. The microcontroller socket [see Fig. 1(a)] introduced a "metal wall" on the PCB which resulted in the shielding of incoming waves originating from certain angles. This influences the isotropic performance of the sensor and as a result, increases the uncertainty.

3) Frequency Verification: Fig. 8 shows the results of the frequency verification test. The SRM-3006 reports every 5 s (rms averaging), meanwhile, the triaxial sensor reports every second. The average E-field reported by both devices for the full test differs by 0.03 V/m or the E-field reported by the triaxial sensor was 0.43 dB higher than the SRM-3006. The maximum difference between the values reported by both devices for a single frequency was 0.3 V/m.

B. Sensor Uncertainty

Three main contributions to the total uncertainty error are the uncertainty error of the calibration device, rms detector, and antenna setup of the sensor (anisotropy). The calibration device has an uncertainty error of ± 3 dB [36]. The uncertainty error of the rms power detector is ± 0.5 dB, depending on the environmental temperature of the detector [31]. The sensor is not fully isotropic, which could result in an underestimation of 5.1 dB [see Fig. 7(b)] or overestimation of 3.8 dB [see Fig. 7(a)]. The relative uncertainty is defined by the ratio of the standard deviation and the average [37]. Following this, the relative uncertainty is 17% for horizontal isotropy and 24% for the vertical isotropy. After combining all contributions, the combined uncertainty error u_c of the sensor is 105% or 3.12 dB. Table III shows an overview of all contributions. The uncertainty of the calibration device has a large contribution to the combined uncertainty.

C. Energy Consumption

The triaxial sensor consumed 0.3 kWh during a period T of six days (measured using an Energy meter). The power draw of the triaxial sensor was also measured by the Energy meter. The triaxial sensor draws 2.1 W of power P. The energy

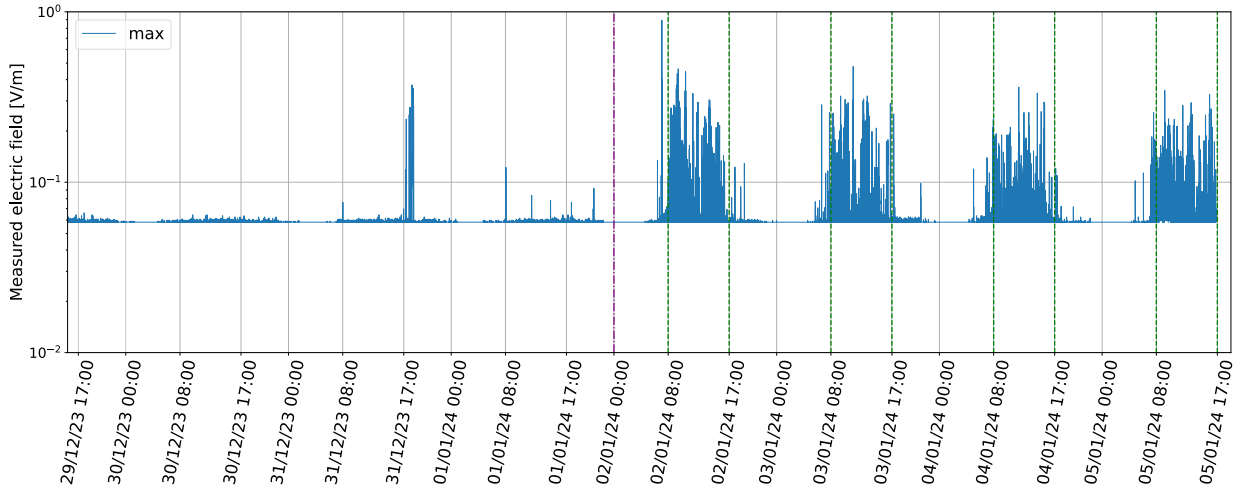

Fig. 9. One week of indoor measurement campaign. The measurement campaign was conducted on the 5th floor of an office building in Ghent, Belgium. The office was closed on days left of the purple dashed line (before January 2nd). The typical working hours of an employee-8 A.M.–5 P.M.-who works at the office are marked by the green dashed lines. The recorded *E*-field levels during the first part of the week are mostly below 0.067 V/m. The maximum recorded *E*-field value during the measurement campaign was 0.89 V/m (1.5% of the maximum allowed *E*-field exposure following the ICNIRP guidelines).

TABLE III
COMBINED UNCERTAINTY u_c OF THE SENSOR

Contribution	Relative uncertainty [dB]	[%]	Ref.
Calibration device	3	100	[36]
Isotropy H	-	17	Fig. 7a
Isotropy V	-	24	Fig. 7b
Power detector	0.5	12	[31]
Combined uncertainty u_c	3.12	105[1]	[37]

[1] $u_c = \sqrt{\sum_i u_i^2}$ with u_i the relative uncertainty of a contribution to the total uncertainty e.g. calibration device

consumption EC_{calc} is also calculated based on the power drawn by the sensors via (4). As a result, the triaxal sensor consumes 0.30 kWh for a period of six days. This translates to an electricity cost of €0.014 per day (the average price for electricity in Belgium is €0.28/kWh)

$$EC_{calc}\,[\text{kWh}] = \frac{P \cdot T\,[\text{hours}]}{1000}. \tag{4}$$

D. In Situ Measurements

Fig. 9 shows the results of the first measurement campaign, which was conducted indoors in an office. The triaxial sensor was measured for 14 days starting on Friday the 22nd of December 2023. The last seven days are discussed because no major traffic was detected in the first week due to the holiday period. The office was closed from the 23rd of December, 2023 until the 1st of January, 2024, hence the low recorded *E*-field values. A day-night pattern can still be observed, left of the purple line on Fig. 9, but the recorded *E*-field values were mostly below 0.067 V/m which is 0.007 V/m above the NF of the sensor (0.06 V/m). The office reopened on the 2nd of January, a region right of the purple line on Fig. 9, hence the increase in activity and thus higher *E*-field values. Every day higher *E*-field values were observed between 8 A.M. and 5 P.M., indicated by the green lines on Fig. 9; this period corresponds to the work regime of most people working at the office. The maximum recorded field is 0.89 V/m, which is ±1.5% of the maximum allowed *E*-field exposure (61 V/m) following the International Commission on Non-Ionizing Radiation Protection (ICNIRP) guidelines [38]. The maximum recorded *E*-field value registered by the triaxial sensor, corresponds to the *E*-field strength of the most energetic OFDM symbol measured during a timeframe of 800 ms.

Fig. 10 and Table IV show the results of the first outdoor measurement campaign, which was conducted in Delft, The Netherlands. Only one user UE was connected to the 5G BS. Four different tests–3 downlink (DL) and 1 uplink (UL)-were conducted. The goal of this measurement campaign is to observe the effect of beamforming toward the user. First, the UE performed a DL test–from now on denoted as DL1–by downloading a 10-GB file repeatedly for a duration of 6 min starting at 11:31 A.M. The UE was positioned in position 1 collinear with the BS and triaxial sensor. The average maximum measured *E*-field was 2.87 V/m (4.8% of ICNIRP limit). Next, the user moved to position 2—where the positions of the sensor, BS, and UE were not collinear—and performed two more DL tests (DL2 and DL3). DL2 started at 12:06 P.M. and DL3 started at 12:12 P.M. The average maximum *E*-field was 7.94 dB lower for DL2 and 7.94 dB lower for DL3 compared to DL1. The sensor was not positioned in the main beam, i.e., the beam from BS toward the UE, but registered *E*-field values above the NF. A value near the NF, as if there was no activity in the cell, was expected but this was not the case. A sidelobe was directed toward the triaxial sensor. The sensor is thus able to measure RF-EMF exposure while not being in the main beam, which indicates that the sensor could be deployed in a monitoring network, although the registered exposure levels would be lower. A single UL test (UL1) was also performed during the measurement campaign. The UE was located in position 1 and at 11:52 A.M., started uploading a 500-MB file to our server, repeatedly. The average maximum amount of *E*-field measured by the sensor was 7.22 dB lower for UL1 compared to DL1. The SRM-3006 was also installed next

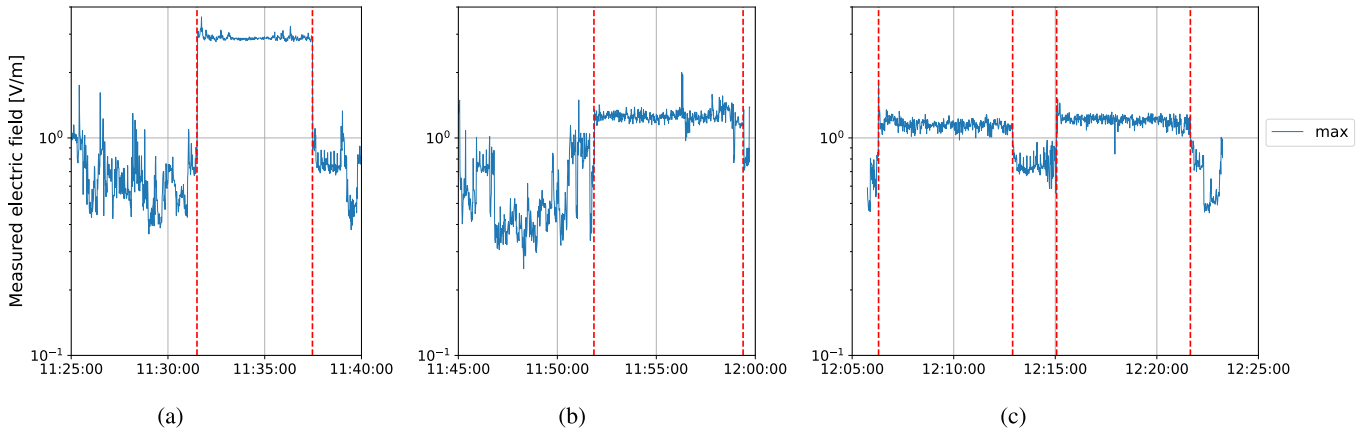

Fig. 10. First outdoor measurement campaign. The measurement campaign was conducted in the Green Village in Delft, The Netherlands. Three DL and one UL tests were performed. DL1 and UL1 were performed when the phone (UE) was in position *P*1 (collinear, same beam). During the DL2 and DL3 tests the phone was present in position *P*2 (noncollinear, out of beam), so lower *E*-field values as in position *P*1 are expected. The maximum *E*-field values measured during the DL1 test were 9.28 dB stronger than during the DL2 test and 7.04 dB stronger than during the DL3 test. (a) DL1. (b) UL1. (c) DL2 and DL3.

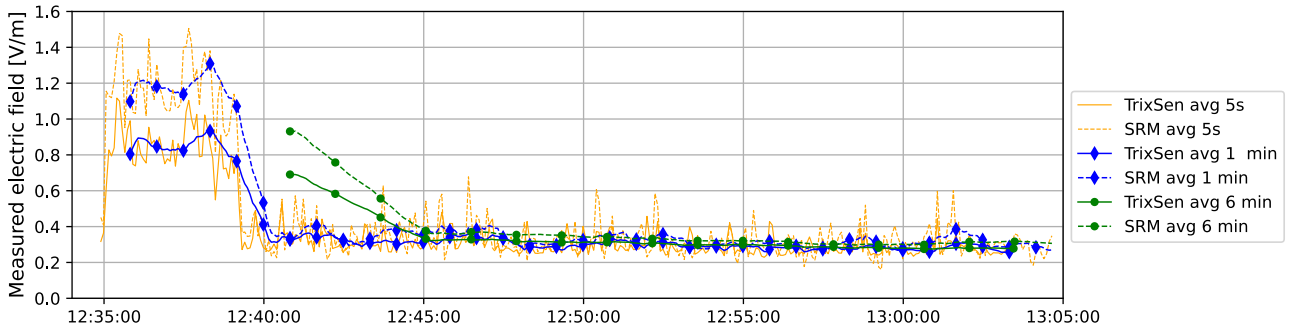

Fig. 11. Second outdoor measurement campaign; the measurement campaign was conducted at a roundabout in Ghent (51.01133°N, 3.70407°E). The DL and ambient *E*-field exposure were measured using the 5G triaxial sensor and SRM-3006, in this figure represented as TrixSen and SRM, respectively. During the file download, the average of the *E*-field values obtained by the triaxial sensor was 2.8 dB lower compared to the results obtained with the SRM. During the second part of the measurement campaign, the average of the *E*-field values obtained by the triaxial sensor was 0.72 dB lower compared to the results obtained with the SRM. The results of both measurements were within the uncertainty range of the SRM, which is a good result.

to the triaxial sensor to compare the obtained ratios. Similar ratios, −9.28 dB for DL2/DL1, −7.04 dB for DL3/DL1, and −7.56 dB for UL1/DL1, were obtained for the average *E*-field measured by the SRM-3006, which was positioned at distance of 2 m from the sensor. The values of the maximum *E*-field obtained by the triaxial 5G sensor cannot be compared to the values of the maximum *E*-field obtained by the SRM. The SRM combines the maximum *E*-field for discrete frequencies for the total duration of a measurement campaign, so these maxima did not occur at the same time. Meanwhile, the triaxial sensor measures the maximum total *E*-field exposure for a wide frequency band, and this is at a higher sample rate than the SRM. The maxima can still be verified by performing spectrum analyzer measurements as seen in [10].

Fig. 11 shows the results of the second outdoor measurement campaign, which was conducted in Ghent. A phone UE was used to download a 10-GB file to generate 5G traffic, and as a result also a beam toward the measurement setup. The final test started at 12:34 P.M. on July 31st. It took the phone 4 min and 20 s to download the file, which corresponds to a continuous throughput of at least 300 Mbit/s. The total duration of the measurement campaign was 30 min. The second part of the measurement campaign lasted for 25 min and was used to measure *E*-field exposure caused by the 5G usage of people driving around the roundabout and by people roaming in the environment of the measurement setup. The results obtained by the 5G triaxial sensor-one sample every second and the SRM-one sample every 5 s—were averaged using a moving average over a period of 5 s, 1 min,

TABLE IV

RESULTS OF THE FIRST OUTDOOR MEASUREMENT CAMPAIGN. THREE DL AND ONE UL TEST WERE PERFORMED BY A USING A SINGLE UE. THE UE WAS LOCATED IN TWO DIFFERENT POSITIONS, FIRST IN POSITION *P*1 AND LATER IN POSITION *P*2. THE TRIAXIAL SENSOR REMAINED IN POSITION *P*1. THE STRENGTH OF THE *E*-FIELD WAS MEASURED AND COMPARED TO THE RESULTS OBTAINED DURING THE FIRST TEST (DL1)

Test	Pos	Start	$E_{max,avg}$ [V/m]	$\frac{E_{max,avg}}{E_{max,avg,DL1}}$ [dB]	$\frac{E_{SRM,avg}}{E_{SRM,avg,DL1}}$ [dB]
DL1	P1	11:31	2.87	–	–
UL1	P1	11:52	1.25	-7.22	-7.06
DL2	P2	12:06	1.15	-7.94	-9.28
DL3	P2	12:12	1.20	-7.57	-7.04

TABLE V
RESULTS OF THE SECOND OUTDOOR MEASUREMENT CAMPAIGN. A DOWNLOAD TEST AND AMBIENT EXPOSURE MEASUREMENT WERE PERFORMED. VALUES OF THE *E*-FIELD WERE MEASURED BY THE TRIAXIAL SENSOR AND THE SRM-3006. THE RESULTS WERE FIRST AVERAGED OVER A PERIOD OF 5 S, 1 MIN, AND 6 MIN AND THEN AVERAGED OVER THE TOTAL TEST DURATION

Device	Download test			Ambient measurement		
	$E_{5\,s\,avg,avg}$ [V/m]	$E_{1\,min\,avg,avg}$ [V/m]	$E_{6\,min\,avg,avg}$ [V/m]	$E_{5\,s\,avg,avg}$ [V/m]	$E_{1\,min\,avg,avg}$ [V/m]	$E_{6\,min\,avg,avg}$ [V/m]
Triaxial Sensor	0.850	0.862	nan[1]	0.299	0.299	0.298
SRM-3006	1.179	1.194	nan[1]	0.325	0.327	0.325

[1] Duration of download test was shorter than 6 minutes.

and 6 min. Next, the results were compared to each other. The average amount of *E*-field exposure during the file download was 0.850 V/m according to the triaxial sensor (TrixSen) and 1.179 V/m according to the SRM. The results obtained with the triaxial sensor are 2.8 dB lower compared to the results obtained with the SRM, which is within the uncertainty of the SRM and thus considered good. The average *E*-field measured by the triaxial sensor during the second part (ambient *E*-field exposure) was 0.299 V/m. Meanwhile, the average *E*-field measured by the SRM was 0.325 V/m, or 0.72 dB higher. A summary of the results can be found in Table V.

IV. SENSOR SPECIFICATIONS AND IMPROVEMENTS

The specifications and capabilities of the sensor are discussed in this section. The cost to produce a sensor, excluding calibration and engineering time, is less than €200. This makes the sensor suitable to be deployed in large monitoring networks. The sensor can be used to observe the temporal behavior of *E*-fields, specifically tailored to 5G. The sensor is capable of measuring *E*-fields stronger than 0.06 V/m for a frequency range that corresponds to the n78 frequency band and the n77 frequency band (up to 3.9 GHz). The combined uncertainty of the sensor is 3.12 dB. The uncertainty of the calibration device has a large contribution to the total uncertainty.

A different free-space calibration technique could improve the calibration and therefore reduce the measurement uncertainty. A different antenna setup is also considered to improve the isotropic behavior sensor of the sensor.

The ADC that is used allows us to sample at the symbol level, which makes it possible to measure the *E*-field exposure related to individual 5G OFDM symbols. This will be tested in situ and extra tests will be performed to verify if the sensor would be able to differentiate between traffic and synchronization signals.

The sensor uses mains power or an external 5 V supply to power the sensor. In the future, batteries (and potentially solar panels) will be used to power the sensor to increase the freedom of future deployments. A real-time clock chip and extra local storage will also be added to the new version of the sensor to make it easier to sync the data and to reduce the network traffic. The latter will also reduce the power consumption of the sensor by reducing the active time of the WiFi modem of the microcontroller.

V. CONCLUSION AND FUTURE WORK

A low-cost triaxial 5G RF-EMF exposure sensor was developed, calibrated, and validated in the field. The sensitivity of the triaxial 5G sensor is 0.06 V/m, while having a combined uncertainty u_c of 3.12 dB. The sensor was tested in situ in one indoor (next to a window) and two outdoor environments (private and commercial 5G network). The maximum measured strength of the *E*-field was 0.893 V/m for the indoor measurement campaign and 2.87 V/m for the outdoor measurement campaign, which are 1.5% and 4.8% of the maximum allowed *E*-field exposure following the ICNIRP guidelines. For the second outdoor measurement campaign, a comparison was made between measurement data obtained by the triaxial 5G sensor and the SRM-3006. The average values of the *E*-field registered by the triaxial 5G sensor differ on average 1.4 dB from these of the SRM-3006.

In the future, more triaxial nodes will be produced to create a 5G monitoring network. Additional capabilities of the simultaneous ADC-based sensor will also be investigated. The simultaneous ADC can theoretically sample the different OFDM symbols used in 5G communication for FR1.

ACKNOWLEDGMENT

This project has received funding from the European Union's Horizon Europe research and innovation programme under grant agreement No 101057262 (GOLIAT). Views and opinions expressed are however those of the authors only and do not necessarily reflect those of the European Union or the Health and Digital Executive Agency. Neither the European Union nor the granting authority can be held responsible for them. The authors would like to thank the Green Village and Sam Aerts for the help during the first outdoor measurement campaign, conducted in Delft, and Javad Heidari for the help during the second outdoor measurement campaign, conducted in Ghent.

REFERENCES

[1] *Technical Specification Group Radio Access Network; NR; User Equipment (UE) Radio Transmission and Reception; Part 1: Range 1 Standalone (Release 18)*, document TS 38.101-1 V18.5.0 (2024-03), 3GPP, 2024.

[2] World Health Organisation. (2020). *Radiation: 5G Mobile Networks and Health*. [Online]. Available: https://www.who.int/news-room/questions-and-answers/item/radiation-5g-mobile-networks-and-health

[3] R. N. Kostoff, P. Heroux, M. Aschner, and A. Tsatsakis, "Adverse health effects of 5G mobile networking technology under real-life conditions," *Toxicol. Lett.*, vol. 323, pp. 35–40, May 2020, doi: 10.1016/j.toxlet.2020.01.020.

[4] F. de Vocht and P. Albers, "The population health effects from 5G: Controlling the narrative," *Frontiers Public Health*, vol. 10, Dec. 2022, Art. no. 1082031, doi: 10.3389/fpubh.2022.1082031.

[5] S. Cucurachi, W. L. M. Tamis, M. G. Vijver, W. J. G. M. Peijnenburg, J. F. B. Bolte, and G. R. de Snoo, "A review of the ecological effects of radiofrequency electromagnetic fields (RF-EMF)," *Environ. Int.*, vol. 51, pp. 116–140, Jan. 2013, doi: 10.1016/j.envint.2012.10.009.

[6] N. Loizeau et al., "Comparison of ambient radiofrequency electromagnetic field (RF-EMF) levels in outdoor areas and public transport in Switzerland in 2014 and 2021," *Environ. Res.*, vol. 237, Nov. 2023, Art. no. 116921. [Online]. Available: https://www.sciencedirect.com/science/article/pii/S0013935123017255

[7] W. B. Chikha et al., "Assessment of radio frequency electromagnetic field exposure induced by base stations in several micro-environments in France," *IEEE Access*, vol. 12, pp. 21610–21620, 2024.

[8] M. R. González, N. F. González, I. López, J. O. Zambrano, A. M. Martínez, and C. M. Unturbe, "Compact exposimeter device for the characterization and recording of electromagnetic fields from 78 MHz to 6 GHz with several narrow bands (300 kHz)," *Sensors*, vol. 21, no. 21, p. 7395, Nov. 2021. [Online]. Available: https://www.mdpi.com/1424-8220/21/21/7395

[9] M. Velghe, S. Aerts, L. Martens, W. Joseph, and A. Thielens, "Protocol for personal RF-EMF exposure measurement studies in 5th generation telecommunication networks," *Environ. Health*, vol. 20, no. 1, pp. 1–10, Apr. 2021, doi: 10.1186/s12940-021-00719-w.

[10] S. Aerts et al., "In situ assessment of 5G NR massive MIMO base station exposure in a commercial network in bern, Switzerland," *Appl. Sci.*, vol. 11, no. 8, p. 3592, Apr. 2021. [Online]. Available: https://www.mdpi.com/2076-3417/11/8/3592

[11] K. Deprez et al., "In-situ 5G NR base station exposure of the general public: Comparison of assessment methods," *Radiat. Protection Dosimetry*, vol. 198, no. 6, pp. 358–369, May 2022, doi: 10.1093/rpd/ncac061.

[12] M. Khuzairi, H. A. Rahim, M. Abdulmalek, and M. N. M. Warip, "Radio frequency radiation measurement for base tower station safety compliances: A case study in Pulau pinang Malaysia," *Bull. Electr. Eng. Informat.*, vol. 8, no. 1, pp. 150–157, Mar. 2019, doi: 10.11591/eei.v8i1.1407.

[13] E. Korkmaz et al., "A comprehensive review of 5G NR RF-EMF exposure assessment technologies: Fundamentals, advancements, challenges, niches, and implications," *Environ. Res.*, vol. 260, Nov. 2024, Art. no. 119524. [Online]. Available: https://www.sciencedirect.com/science/article/pii/S0013935124014294

[14] C. Apostolidis, A. Manassas, S. Iakovidis, and T. Samaras, "Electromagnetic fields in the environment: An update of monitoring networks in Europe," in *Proc. 3rd URSI Atlantic Asia Pacific Radio Sci. Meeting (AT-AP-RASC)*, May 2022, pp. 1–3.

[15] S. Aerts et al., "Lessons learned from a distributed RF-EMF sensor network," *Sensors*, vol. 22, no. 5, p. 1715, Feb. 2022. [Online]. Available: https://www.mdpi.com/1424-8220/22/5/1715

[16] K. Deprez et al., "Comparison of low-cost 5G electromagnetic field sensors," *Sensors*, vol. 23, no. 6, p. 3312, Mar. 2023, doi: 10.3390/s23063312.

[17] F. Minucci et al., "Measuring 5G electric fields strength with software defined radios," *IEEE Open J. Commun. Soc.*, vol. 3, pp. 2258–2271, 2022.

[18] A. Sârbu, M. D. Migliore, E. Şorecău, M. Şorecău, S. Miclăuş, and P. Bechet, "SDR-enabled multichannel real-time measurement system for in situ EMF exposure evaluation," *Electronics*, vol. 11, no. 17, p. 2670, Aug. 2022, doi: 10.3390/electronics11172670.

[19] L. Tuta, F. Panait-Radu, F. Ardelean, D. Gorgoteanu, and G. Rosu, "SDR-based portable system for evaluating exposure to ambient electromagnetic fields," *Electronics*, vol. 12, no. 24, p. 5003, Dec. 2023, doi: 10.3390/electronics12245003.

[20] *EXEM*. Accessed: Jan. 6, 2025. [Online]. Available: https://www.exem.fr/

[21] *Agence Nationale Des Fréquences. Observatoire Des Ondes*. Accessed: Jan. 6, 2025. [Online]. Available: https://www.anfr.fr/maitriser/information-du-public/observatoire-des-ondes

[22] *Observatoire Des Ondes. Observatoire Des Ondes*. Accessed: Jan. 6, 2025. [Online]. Available: https://www.observatoiredesondes.com/

[23] EMF Ratel. *EMF Level Monitoring*. Accessed: Jan. 6, 2025. [Online]. Available: https://emf.ratel.rs/

[24] *Monitor EMF*. Accessed: Jul. 16, 2024. [Online]. Available: https://www.monitor-emf.ro/map

[25] Monitor. stations. *National Oberservatory of Electromagnetic Fields*. Accessed: Jan. 6, 2025. [Online]. Available: https://paratiritirioemf.eeae.gr/index.php/en/measurements/map

[26] EMF Ratel. *National Network for Monitoring the Non-Ionizing E / M Radiation of Wireless Telecommunication Systems*. Accessed: Jan. 6, 2025. [Online]. Available: https://pedion24.gr/

[27] *Narda–Safety Test Solutions. AMB-8059*. Accessed: Oct. 10, 2024. [Online]. Available: https://www.narda-sts.com/en/products/emf-24/7-area-monitor/amb-8059/

[28] Narda–Safety Test Solutions. *AMB-8059, Continuous, Remote Monitoring and Logging of Electromagnetic Fields*. Accessed: Jan. 14, 2025. [Online]. Available: https://www.narda-sts.com/index.php?eID=dumpFile&t=f&f=1176&dl=1&token=66a921918cbade9f8d678c5f121a6f5477ccc8a8

[29] Wavecontrol. *MonitEM RF Area Monitor*. Accessed: Oct. 10, 2024. [Online]. Available: https://www.wavecontrol.com/rfsafety/en/products/area-monitors-monitem/monitem

[30] Wavecontrol. *Monitem*. Accessed: Jan. 14, 2025. [Online]. Available: https://www.wavecontrol.com/rfsafety/images/data-sheets/en/MonitEM_Datasheet_EN.pdf

[31] *HMC1120, RMS Powers Detector & Envelope Tracker, DC-3.9 GHz*. Accessed: Nov. 16, 2023. [Online]. Available: https://www.analog.com/en/products/hmc1120.html

[32] E. Dahlman, S. Parkvall, and J. Sköld, "Initial access," in *5G NR: The Next Generation Wireless Access Technology*. New York, NY, USA: Academic, 2018, ch. 16, pp. 311–334. [Online]. Available: https://www.sciencedirect.com/science/article/pii/B9780128143230000168

[33] Ansmann. *Hc105*. Accessed: Jan. 24, 2025. [Online]. Available: https://shop.ansmann.de/en/home-charger-hc105-black

[34] C. A. Balanis, *Antenna Theory: Analysis and Design*. Hoboken, NJ, USA: Wiley, 2015.

[35] Narda–Safety Test Solutions. *SRM-3006—Frequency-Selective EMF Measurement Up to 29.5 GHz*. Accessed: Jan. 6, 2025. [Online]. Available: https://www.narda-sts.com/en/products/emf-selective-measuring-devices/srm-3006/

[36] *Edition 2.0 2019/04-Case Studies Supporting IEC 62232–Determination of RF Field Strength, Power Density and SAR in the Vicinity of Radiocommunications Base Stations for the Purpose of Evaluating Human Exposure*, Standard IEC 62669, 2022.

[37] Univ. North Carolina. *Introduction to Measurements & Error Analysis*. Accessed: Jan. 28, 2025. [Online]. Available: https://astro.pas.rochester.edu/~aquillen/phy141/lectures/pdfs/uncertainty_nc.pdf

[38] G. Ziegelberger et al., "Guidelines for limiting exposure to electromagnetic fields (100 kHz to 300 GHz)," *Health Phys.*, vol. 118, no. 5, pp. 483–524, 2020, doi: 10.1097/HP.0000000000001210.

Jeroen Van der Straeten received the M.Sc. degree in electrical engineering: electronic circuits and systems from Ghent University, Ghent, Belgium, in 2023, where he is currently pursuing the Ph.D. degree with the WAVES-IMEC Research Group, Department of Information Technology, IMEC.

His research interests include the design of sensors to measure radio frequency electromagnetic (RF-EMF) exposure induced by 5G telecommunication for FR1 and FR2. He is also interested in automated RF-EMF measurement setups.

Han Van Bladel received the M.Sc. degree in electronics and information and communication technologies (ICT) engineering technology from Ghent University, Ghent, Belgium, in 2022, where he is currently pursuing the Ph.D. degree with the WAVES Research Group, Department of Information Technology.

His research interests include the design of sensors to measure radio frequency electromagnetic (RF-EMF) exposure.

Kenneth Deprez received the M.Sc. degree in electronics and information and communication technologies (ICT) engineering technology from Ghent University, Ghent, Belgium, in 2019, where he is currently pursuing the Ph.D. degree with the Wireless, Acoustic, Environment, and Expert Systems (WAVES) Group, Department of Information Technology.

In September 2019, he joined the WAVES Group, Department of Information Technology, Ghent University. His current research interests include monitoring networks for electromagnetic fields-extremely low frequency (EMF-ELF), EMF-radio frequency (EMF-RF), and mm-waves and positioning and sensing based on visible light (VLP/VLS).

Wout Joseph (Senior Member, IEEE) was born in Ostend, Belgium, in October 1977. He received the M.Sc. degree in electrical engineering from Ghent University, Ghent, Belgium, in July 2000, and the Ph.D. degree from Ghent University, in March 2005.

His Ph.D. work dealt with measuring and modeling of electromagnetic fields around base stations for mobile communications related to the health effects of exposure to electromagnetic radiation. From 2007 to 2012, he was a Postdoctoral Fellow at the Research Foundation Flanders (FWO-V), Brussels, Belgium. Since October 2009, he has been working as a Professor of Experimental Characterization of Wireless Communication Systems. He has been working as a PI with IMEC, Ghent, since 2017. His professional interests include electromagnetic field exposure assessment, propagation for wireless communication systems, antennas, and calibration. Furthermore, he specializes in wireless performance analysis and quality of experience.

Günter Vermeeren is working as a Professor with the WAVES Research Group, Department of Information Technology, IMEC, Ghent University, Ghent, Belgium, where he is involved in the research on radio frequency dosimetry, electromagnetic exposure, and on-body propagation. He is the author of 57 publications in international journals and 54 papers at national and international scientific conferences. His research interests include numerical modeling (FDTD, MoM) as well as measurements of electromagnetic fields in the proximity of humans (exposure as well as on- and in-body propagation). His research results are also included in the international standard IEC 62232. Since 2013, he is also involved in research on medical imaging systems with a focus on the modeling of the electromagnetic fields in hybrid MRI systems.